ACCELERATION, TRANSPORT OF AND RADIATION BY ELECTRONS IN IMPULSIVE PHASE OF FLARES

Vahé Petrosian
Center for Space Science and Astrophysics and
Department of Applied Physics
Stanford University
Stanford, CA 94305
USA

ABSTRACT. I review here results of works that we have carried out over the past few years in connection with various manifestations of the impulsive phase of solar flares. The primary goal of this work has been the determination of the characteristics of the accelerated electrons. We take into account various possible interactions that electrons suffer as they traverse the flare plasma and evaluate the expected radiation via several mechanisms. The comparison of these with the observed x-ray, gamma-ray and radio emissions allows us to set constraints on the characteristics of the accelerated electrons and on some properties of the flare plasma. I will describe some of the results we have derived from comparisons with SMM and other observations of flares during the past solar cycle. In particular, I will show that we can set limits on the range and distribution of the accelerated electron spectrum and pitch angle distribution, and on the column depth and field convergence rate of the flaring loop. More complete data and high spatial resolution and polarization observations could be very useful for furthering this kind of work.

I. INTRODUCTION

It is generally agreed that the source of energy of flares is current carrying magnetic fields, but the exact mechanism of release of energy and acceleration of particles remains the central and unsolved problem of solar flares. There has been, however, considerable progress in determination of the characteristics of the flare radiation and physical parameters of the models. In particular, it is now generally accepted that the bulk of the radiation observed during the impulsive phase of flares is either due to direct emission by accelerated electrons and ions (primarily protons) or is the result of deposition of energy of the accelerated particles in the flare plasma.

The analysis and interpretation of these radiations, therefore, are the first important steps in learning about the characteristics of the accelerated electrons. X-ray and continuum gamma-ray radiation, which are believed to be due to bremsstrahlung provide the most direct information in this regard, especially in the thick target model which, as we show below, is the most viable model. The primary uncertainties in the analysis of these data arise from our lack of knowledge about the magnetic field topology (assumed generally to be in the form of loops of magnetic flux), the plasma density and the variation of these quantities along the loop. These uncertainties become more severe in the case of microwave

E. R. Priest and V. Krishan (eds.), Basic Plasma Processes on the Sun, 391–402.

and type III emissions, which are also intimately connected with the impulsive phase. The analysis of these radiations requires a knowledge of the strength of the magnetic field, a more precise idea about acceleration site with respect to the flaring loop and other field lines, and inclusion of effects due to electron beam-plasma wave dynamics as well as radiation transport effects (optically thick or thin emission).

The whole problem is further complicated because the radiative processes are not the main mechanisms of dispersion and energy loss for the electrons. Coulomb collisions dominate for high density plasmas and low energy particles. Synchrotron losses become important at higher particle energies and field strengths for lower plasma densities. And the degree of loss due to plasma wave-particle interactions is quite uncertain. This means that the radiation does not reflect the characteristics of the initially accelerated particles, but their characteristics after they are modified by the above interactions. It is, therefore, imperative that the particle transport is taken into account properly.

In a series of papers with various graduate students at Stanford, we have been carrying out a systematic study of the above kinetic and radiative processes. In the next section I will summarize some of these theoretical studies. I will outline the process of comparison of these models with observations in section III, and in section IV, I will present some results and conclusions that we reach from such comparisons.

II. KINETIC EQUATION AND BASIC MODEL

In most astrophysical plasmas, and in particular, for solar flare plasmas, the gyroradius of the particles about the magnetic field is many orders of magnitude less than other length scales in the problem. Thus, the charged particles are essentially tied to the magnetic field lines so that the distribution function in phase space can then be specified by the position along the field lines and two components of momentum (or energy and pitch angle with respect to the magnetic field). The particle density distribution function $f(E,\mu,s,t)$ is then a function of four variables, the kinetic energy $E=\gamma-1$ (expressed in units of mc^2), the pitch angle α (or $\mu=\cos\alpha$), the position s along the field, and the time t. In the limit where the change in particle momentum due to individual scatterings is much less than the original momentum, we can make use of the Fokker-Planck expansion of the Boltzmann collision integral in the continuity equation for f (see e.g. Lifshitz and Pitaevskii 1981). The Fokker-Planck equation can then be written in the form

$$\frac{\partial f}{\partial t}=-\mu c\beta\frac{\partial f}{\partial s}-\frac{\partial}{\partial\mu}(\dot{\mu}f)-\frac{\partial}{\partial E}(\dot{E}f)+\frac{\partial}{\partial\mu}(D_{\mu\mu}\frac{\partial f}{\partial\mu})+\frac{\partial}{\partial E}(D_{EE}\frac{\partial f}{\partial E})+$$
$$\frac{\partial}{\partial E}(D_{E\mu}\frac{\partial f}{\partial\mu})+\frac{\partial}{\partial\mu}(D_{E\mu}\frac{\partial f}{\partial E})+S(E,\mu,s,t), \qquad (1)$$

where βc is the velocity and $S(E,\mu,s,t)$ is the source. The coefficients $\dot{E}$ and $\dot{\mu}$ are the systematic changes in energy and pitch angle cosine due to external forces, radiation, and scattering, while the diffusion coefficients D_{ij} are due only to scattering processes. Note that the diffusion coefficients are defined differently than in the usual Fokker-Planck formalism.

https://doi.org/10.1017/S0074180900088306 Published online by Cambridge University Press

a) The Interactions. The forms of $\dot{E}$, $\dot{\mu}$, and D_{ij} due to interactions of electrons with the ambient plasma particles, waves and magnetic field, and due to external forces have been published in various publications and are summarized in Hamilton, Lu and Petrosian (1990). Here we briefly mention some important features of these interactions.

Coulomb Collisions: Leach and Petrosian (1981), and Leach (1984) give these coefficients for different compositions and for partially ionized plasmas. We consider energies $E < 10^4$ so that *bremsstrahlung* losses are always less than Coulomb losses.

Magnetic Mirroring: Systematic change in the pitch angle occurs due to variation of the magnetic field B and is calculated using the adiabatic invariance of flux through particle orbits (see McTiernan and Petrosian 1990a, and McTiernan 1989).

Synchrotron: Classical optically thin synchrotron emission is assumed so that there are no diffusion terms (see e.g. Petrosian 1985).

External Forces: We ignore drifts perpendicular to the magnetic field (McTiernan 1989) so that only the component of the force parallel to the magnetic field $F_{\|}$ needs to be considered.

Plasma Turbulence: The diffusion rates due to the scattering of electrons by fluctuations in the magnetic or electric fields (Alfvén or Langmuir waves) are taken mainly from Schlickeiser (1989) and are given in Hamilton et al (1990).

We do not consider *Inverse Compton* losses which are expected to be unimportant for solar flare conditions, or the effects of the *Reverse Currents* which when important lead to the destruction of the nonthermal beams of electrons, that are needed for production of most of the observed radiations.

b) The Source Term. The source term $S(E, \mu, s, t)$ describes the characteristics of the accelerated electrons. As a starting point, we make the simplest assumption that this is a separable function of its parameters: $S(E, \mu, s, t) = F(E)G(\mu)H(s)K(t)$. There is a strong indication that the energy spectrum can be approximated by a power law with a spectral index δ : $F(E) = F_T(\delta - 1)(E/E_o)^{-\delta}/E_o$, where F_T is the total flux above energy E_o. For the pitch angle distribution we assume a gaussian form which peaks in a direction α_1 (or μ_1) and has a width α_o (or μ_o). The pitch angle distribution becomes important when we deal with anisotropic emission processes and observations with information about the directivity of the radiation. In general, we take $\alpha_1 = 0$ which means that the accelerated electrons are beamed along the magnetic lines of force, but in some cases we also use what we call pancake distributions with $\alpha_1 = \pi/2$. Values of $\alpha_o \gg \pi/2$ represent the isotropic distribution.

We have little direct information about the spatial distribution of the accelerated electrons except that the acceleration must occur above the transition region in the corona. We shall assume that the injection of the accelerated electrons occurs near the top of a symmetrical loop. Because most of the observations that we shall be concerned with are spatially unresolved, the exact spatial distribution is not important. Therefore, for simplicity, we assume a delta function injection $H(s) = \delta(s - s_o)$ with $s_o = 0$ corresponding to injection at the apex of the loop. For the time dependence we make two extreme assumptions depending on the observations. For observations with time resolution (or observed intensity variation

https://doi.org/10.1017/S0074180900088306 Published online by Cambridge University Press

time scale) much greater than the interaction time scale, or the time taken by the electrons to traverse the whole length of the loop ($\simeq$ 0.1 s), we assume the steady state condition: $\partial f/\partial t = 0, K(t) =$ constant. In this case, the observed variations reflect directly the form of $K(t)$ up to the resolution of the observation. In the opposite limit, for treating high time resolution observations or rapid fluctuations, one must include the $\partial f/\partial t$ term. In general, for these cases, we initially assume impulsive injection at time t_o; $K(t) = \delta(t - t_o)$.

c) The Plasma. We assume a cold plasma so that the only plasma parameters we need to specify are the values of the plasma density and magnetic field along the whole length of the loop: $n(s)$ and $B(s)$. The two most important parameters are the column depth to transition region at $s = s_{tr}$; $N_{tr} = \int_o^{s_{tr}} nds$, and the rate of the convergence of the magnetic field, $d\ln B/ds$, in the corona for low energy particles and in the photosphere for higher ones. We shall sometimes use the mirror ratio which is the ratio of magnetic field at $s = 0$ to that at the "end" of the loop: $b = B_o/B_{max}$. For low energy particles $B_{max} \approx B_{tr}$ but for higher energies, it may be as large as the field at the photosphere. For higher energy particles, the synchrotron losses and pitch angle scattering by plasma waves become important. In this case we need the absolute value of the magnetic field and the plasma wave density.

Analytic solutions have been obtained for equation (1) for some restricted problems, in particular, for small pitch angles (Leach and Petrosian 1983, Leach 1984, and Lu and Petrosian 1988) and for extremely relativistic electrons suffering Coulomb collision and synchrotron losses (McTiernan and Petrosian 1990a). Numerical codes for solution of the steady state equation were first developed by Leach (1984) and have been extended by McTiernan (1989) to higher energies and field strengths, and for the general time dependent problem by Hamilton, Lu and Petrosian (1990). The results described in the next two sections are based on all of these solutions.

III. COMPARISON WITH OBSERVATIONS

Using the results from the Fokker-Planck equations, we calculate the characteristics of the expected radiations from the resultant electron distribution. Comparison with observations then allows us to determine the characteristics of the accelerated electrons (parameters $F_T, \delta, E_o, \alpha_1, \alpha_o$) and of the plasma ($N_{tr}, d\ln B/ds$ or the mirror ratio b),in addition to testing the validity of our assumptions related to the source term S and the loop model. In general, such a comparison can be done in two different ways. In one, which is generally useful in the initial stages of investigation of a phenomenon, a few strong and well observed events are studied in great details. This approach, the most commonly used one, especially with observation from SMM, has proven the reliability of the non-thermal thick target model as described above and has shown that most of the model parameters have very wide ranges (sometimes having pure power law distributions indicating indefinite range). This then demands the second approach, whereby from statistical analysis of the observed properties of a large number of events, one attempts to describe the distribution of (or occurrence rate of flares with) various parameters, which can be written as $\psi_e(F_T, \delta, \alpha_i)$,

https://doi.org/10.1017/S0074180900088306 Published online by Cambridge University Press

where α_i stands for $\alpha_1, \alpha_n, d\ln B/ds, N_{tr}$, etc.

This, of course, is an ambitious goal. However, there are sufficient channels and modes of observations so that, in principle, this is an achievable goal. The impulsive phase of flares can be studied through spectral, temporal, spatial and polarization observations of hard x-ray, gamma-ray, microwave at type III emissions. The first two aspects of these emissions have been observed extensively but there is very little data with high spatial resolution (some at low energy x-rays from HXiS on SMM and from Hinotori, and some from VLA; for a review see the proceedings of the SMM workshop, Kundu and Woodgate, 1985) and there is essentially no reliable data on polarization (except for few flares at microwaves and possibly one flare at low hard X-rays; see Leach, Petrosian and Emslie, 1985, and references cited there). We will present results from both kinds of comparisons with observations. This, by no means, will be a complete description because the space limitation will not allow us to describe all of our results and, more importantly, results from similar studies by many other workers in the field.

IV. RESULTS AND CONCLUSIONS

We now compare the models with various observations with the aim of setting constraints on the parameters and their distributions.

a) Hard X-rays. We start with analysis of flare emission from 20 to 300 keV which is due to electron bremsstrahlung. This is the energy range where there has been the most systematic observation with those from HXRBS providing the largest set of high quality data. For a recent review see Dennis (1988) and the references there. These data are consistent with the non-thermal thick target model and, in general, show a power law spectrum: $J_x(k) \propto k^{-\gamma}$. There is no strong evidence for correlation between the photon flux J_x and spectral index γ. The distribution of x-ray fluxes(or photon counts) is observed to be a power law: $\psi_x(J_x) \propto J_x^{-1.8}$, approximately in agreement with earlier observation (Datlowe, Elcan and Hudson 1974). On the other hand the distribution of spectral indices has a finite range and is peaked at $\gamma \simeq 4$ (see figure 1).

It is well known, and our calculations confirm, that in the thick target model the hard x-ray emission is nearly isotropic and that its flux integrated over angles and space, $J_x(k) \propto F_T$, the electron flux, and that the index $\gamma = \delta + 1 + \epsilon(\theta, \delta)$, where ϵ and its derivatives with respect to δ or direction of observation θ are $\ll 1$. We can immediately conclude that the distribution of the accelerated electrons, $\psi_e(F_T, \delta, ...) \propto F_T^{-1.8} h(\delta)$. Then using model calculations we derive a form of $h(\delta)$ (the dashed line in figure 1) which gives the solid line x-ray spectral distribution in agreement with the observed histogram. Moreover, extending these results to bremsstrahlung at higher energies (300 keV and 1 Mev), we evaluate the expected distribution of HXRBS fluxes and spectral indices of the subset of these flares which could also be detected by GRS on SMM and find good agreement with the observations as shown by the lower histogram in figure (1). The details of these results

https://doi.org/10.1017/S0074180900088306 Published online by Cambridge University Press

can be found in J. McTiernan's thesis (1989) or in McTiernan and Petrosian (1991).

b) Gamma-rays (> 300 keV). For most flares the gamma-ray spectrum in the range between 1 to 7 MeV is dominated or contaminated by nuclear line emission. Therefore, we have considered the range between 300 keV to 1 Mev and that > 10 Mev separately. The choice of the lower limit is arbitrary and is chosen to correspond to the threshold of the GRS on SMM. As pointed out earlier (Petrosian, 1985) as we go to higher energies, the calculations and, therefore, the interpretation of the data is simplified gradually in three respects. At higher energies (i) the pitch angle diffusion rate of electrons due to collision (or other processes) becomes less important relative to energy loss rate, (ii) the photon is emitted in the direction of momentum of the electron, and (iii) most of the radiation comes from deeper layers, certainly below the transition region, where the field lines will be most likely vertical (or at least have uniform direction). Because of these the gamma-rays will reflect the characteristics of the accelerated electrons more clearly than hard x-rays, for which most of these characteristics are obscured by collisional diffusion and spatial inhomogeneities. However, other consequences of the above mentioned differences is that the degree of convergence of the field lines begins to play an important role and two other complications come in at very high energies. These are the energy losses due to the synchrotron process, which can be accounted for easily (McTiernan and Petrosian 1990a), and the possibility of pitch angle diffusion by plasma turbulence (Miller and Ramaty 1989, and Hamilton, Lu and Petrosian 1990), which requires some knowledge about the type, spectrum and energy density of turbulence that may be present in the flare plasma.

We shall not consider the effects of turbulence which are quite uncertain but include all other processes in a steady state calculation of the spectrum and directivity of the spatially integrated gamma-rays. We assume the distribution of the electron fluxes and spectral indices derived above and vary the parameters α_i from model to model. Of these parameters the most important are the gaussian width of the pitch angle distribution and the rate of the convergence of the magnetic field as long as the column depth $N_{tr} \leq 10^{22}\mathrm{cm}^{-2}$. We have used beamed, isotropic and pancake distributions and two models for field convergence. In one, we assume $d\ln B/ds =$ constant, which emphasizes the field convergence in the corona. In the other, which emphasizes the convergence below the transition region, we set $B \propto n^{\epsilon}$ with $\epsilon = 0.2$. Note that equapartition or a constant β plasma would mean $\epsilon = 0.5$ because the temperature below the transition region is relativly constant.

The anisotropy of the expected radiation is compared with observations. The direct observation of the anisotropy via stereoscopic observations (Kane it et al. 1988) unfortunately suffer from large uncertainties and are not useful for constraining the models. Nevertheless they are consistent with the basic model (McTiernan and Petrosian, 1990b). More conclusive but indirect evidence has come from GRS on SMM which has discovered considerable center-to-limb variation (Vestrand *et al.* 1987) specially for flares with emission at > 10 Mev photon energies (Rieger *et al.* 1984). As emphasized before (Petrosian, 1985), interpretation of this kind of data requires a statistical analysis and therefore a knowledge of

the distributions of the parameters. With the distributions derived above we now have the proper tools for analysis of this kind of data.

I would also like to emphasize that it is important to carry out the appropriate kind of analysis depending on the type of the distribution under consideration and the sensitivity or threshold of the observations. For example, consider a characteristic X with the distribution $\psi(X) \propto X^{-\alpha}$ that is known to be anisotropic, $X = X_o f(\theta)$. Two simple properties of a sample of events (for which X is known) are the variation with θ of the total number and average value of X:

$$N(\theta) = \int_{X_{th}}^{\infty} \psi(X(\theta))dX, \quad \overline{X}(\theta) = \int_{X_{th}}^{\infty} X\psi(X(\theta))dX/N(\theta) \tag{2}$$

where X_{th} is the threshold value for detection of X. It is easy to show that if $X_{th} > X_{min}$, where X_{min} is the minimum value (or the lower cutoff) of the real distribution $\psi(X)$, then $\overline{X}(\theta)$ = constant but $N(\theta) \propto [f(\theta)]^{1-\alpha}$. In the opposite case $N(\theta)$ =constant and $\overline{X}(\theta) \propto f(\theta)$, irrespective of whether $\psi(X)$ has a power law form or not. In the first case $N(\theta)$ and in the second case $\overline{X}(\theta)$ is the parameter that will reflect the anisotropy. Therefore, it is important to make the correct test.

As shown in McTiernan and Petrosian (1990b), as we go to higher energies, both flux and spectral index show stronger dependence on the angle of observation with respect to the field lines (which for vertical field lines is the same as the heliocentric longitude). Figure 2 shows these effects for some models. However, as we have seen in section II above, the distribution of fluxes has a power law form extending beyond the threshold of HXRBS and GRS so that in this case we must look at the center-to-limb variation of the number of flares and not that the average value of the flux. On the other hand because the distribution of spectral index appears to turn over at both high and low values in this case we deal with the center-to-limb variation of the average value of the spectral index. It should be noted that there may be some instrumental effects in thsee distribution, but we ignore them as they are considered to be secondary effects.

The first result we obtain is that the center-to-limb variation of N in most models agrees with observations, but the calculated average spectral index shows the same general trend as the observations (spectral flattening toward the limb) but has a larger absolute value than those observed by GRS on SMM (i.e. the model spectra are steeper). This forces us to alter our assumption that the electron spectrum is described by a single power law at all energies. Instead there must be a brake (or gradual flattening) around 300 keV. This statistical evidence has been seen in spectra of individual flares (Dennis, 1988) and in spectra of impulsive electron flares observed directly at one A.U. (Dröge *et al.*,1989).

We then include such a break and from comparison of the center-to-limb variation of the spectral index, the ratio of HXRBS to GRS fluxes and the number of flares we place limits on the range of two of our model parameters mentioned above. These limits are shown in

https://doi.org/10.1017/S0074180900088306 Published online by Cambridge University Press

figure (3) which clearly rules out pancake models but allows beamed models with various degrees of beaming (value of α_o). The allowed values are anti-correlated with the degree of field convergence (the mirror ratio b) such that the stronger the convergence, the smaller α_o or the stronger the beaming. A narrower range is found from the spectral index data than from the ratio of fluxes. The distribution of the flares with emission at > 10 Mev across the solar disk also can be reproduced by the models in the allowed region of the diagram. The details of these results can be found in McTiernan (1989) and McTiernan and Petrosian (1991).

c) Microwaves. The microwaves are believed to be due to the synchrotron emission by the same population of electrons that produces the hard x-rays because of the correlation between the fluxes and similarity of the time profiles of the emission at the two energy bands. Many authors have discussed the relative number of electrons needed for production of x-rays and microwaves (Peterson and Winkler 1959, Takakura and Kai 1966, Holt and Ramaty 1969, Gary 1985, Schmahl, Kundu and Dennis 1985, and Kai 1986) with different conclusions. Some of these differences are due to the use of different models (e.g., thin target vs thick target) or due to effects of absorption of the synchrotron radiation. It turns out that the predicted ratio of hard x-ray to microwave emission (at high frequencies where absorption effects can be neglected) is sensitive to the x-ray spectral index γ (or electron index δ) and has different dependence on γ for different models.

In a recent paper (Lu and Petrosian 1989), we have used this fact and compared with observations the prediction of the thick target, thin target and thermal (multi-temperature so that one obtains a power law x-ray spectrum) models. From this we conclude that the model most consistent with observation is the thick target model with loop length of $\simeq 2 \times 10^9$ cm and average magnetic field strength of 500 to 350 G. In the thick target model the same population of electrons produce both radiation but from different locations. The microwaves come from the coronal portion of the loop where the electron spent most of their lifetime (essentially like in a thin target model) while the x-rays originate primarily from the footpoints and below the transition region where the density is higher and where the lifetime of electrons is proportionately lower. This picture essentially agrees with the existing but limited high spatial resolution observations mentioned above (Canfield *et al.*, 1985). On the other hand this difference between the sites of emissions of the two radiations may imply existence of differences in their temporal evolutions.

We have investigated this problem using the time dependent code mentioned above in the framework of the thick target model just described (Lu and Petrosian 1990). Two types of differences have been observed. On time scales comparable to electron transport time, it has been observed that elementary impulsive spikes peak later by about a quarter of a second at microwave as compared to x-rays, while one would expect the microwave emission coming from the the top of loop to start earlier than the x-rays which come from the footpoints. However, if the magnetic field converges from the top to the footpoints of the loop, some of the particles will be trapped in the corona and continue to emit synchrotron

radiation for a longer time. We show that delays of up to 200 millisecond are possible by this method. For longer delays we must change our basic assumption that all energy particles are accelerated with the same time profile. The higher energy, microwave emitting, electrons must be accelerated later than the lower energy, x-ray emitting, ones: For example $K(t) = \exp[-((t + 0.1 - 0.3\beta)/0.07)^2]$ results in delay of microwaves with respect to the x-rays by 350 milliseconds.

Another kind of observed difference between the two time profiles is that on longer time scales the microwaves, on average, peak about 2 seconds later than x-rays and that during the decay phase of the burst there is excessive microwave emission as compared to x-rays. We find that contribution to microwaves from other radiative processes (such as free free or thermal synchrotron), or even very strongly converging field geometries (for trapping of the electrons in the corona) fail to explain the observation with reasonable parameters. Thus we tentatively conclude that these observations are an indication of hardening of the accelerated electron spectra (e.g. change into a flatter power law at higher energies) during the latter stages of an impulsive burst.

It would be useful to make a similar comparison between the gamma-ray and microwave emissions which are produced by electrons with similar energies.

d) Other Processes. We have also studied other flare associated processes, specially those involving wave particle interactions. Because of space limitations I will not describe these in any detail here. We can analyze the effects on the transport of the electrons due to interaction with plasma particles, waves and converging fields simultaneously, an important improvement on past works in flares. For example, we have generalized (Hamilton and Petrosian, 1990) the work by White, Melrose and Dulk (1986) on the possibility of maser action by inclusion of the effects of collisions explicitly. We find that even at moderate column depths to the transition region, $N_{tr} \simeq 2 \times 10^{19}\text{cm}^{-2}$, the electron velocity distribution becomes smoothe reducing the magnitude of the possible maser action.

In a preliminary study we have also evaluated the expected spectral distribution of stochastically accelerated electrons when the ambient plasma has finite density. We find that presence of collisions can produce the type of observed spectral brakes discussed above. This possibility was also demonstrated analytically by Steinacker, Dröge, and Schlickeiser (1988) in connection with the observed brakes in the spectrum of the interplanetary electrons mentioned above(Dröge *et al.*, 1989). These results could also explain the observed hardening of accelerated electron spectra at higher energies (item b) or at later times in the evolution of the impulsive phase (item c). These are preliminary results and more data and theoretical work is needed for the clarification of these important points.

5) Summary. In summary, we have demonstrated that important conclusions about the properties of the acceleration process and about the flare plasma can be reached by the type of analysis we have been engaged in. Some of these are: (i) distribution of fluxes

https://doi.org/10.1017/S0074180900088306 Published online by Cambridge University Press

and spectral indices of accelerated electrons, (ii) deviation from simple power law energy spectrum at higher energies, (iii) spectral hardening during the later stages of the impulsive spikes of long and short durations, (vi) limits on the possible range of th pitch angle distribution of the electrons, and (v) limits on the length, density and field convergence rate of flaring loops.

Acknowledgement: All of the results I have described above are outcomes of the thesis research of Russell Hamilton, Edward Lu and James McTiernan. I would like to thank J. McTiernan for help in the preparation of the figures and specially R. Hamilton for extensive help in the preparation of this manuscript. Our research on solar flares has been supported by NASA grant NAGW 1976 and NSF grant ATM 8705084.

REFERENCES

Canfield,R. et al, 1985, **Energetic Phenomena on the Sun**. Eds. M.R. Kundu and B. Woodgate, NASA Conf. Publ. 2439, Chapter 3.

Datlowe, D.W., Elcan, M.J. and Hudson, H.S. 1974, *Solar Phys.*, **39**, 155.

Dennis, B.R. 1988, *Solar Phys.*, **118**, 49.

Dröge, W., Meyer, P., Evanson, P., and Moses, D. 1989, *Solar Phys.*, **121**, 95.

Gary, D. 1985, *Ap.J.*, **297**, 799.

Hamilton, R.J., Lu, E.T., and Petrosian, V. 1990, (To be published in *Ap.J.* May 10, 1990).

Hamilton, R.J. and Petrosian, V. 1990, (Submitted to *Ap.J.*).

Holt, S. and Ramaty, R. 1969, *Solar Phys.* **8**, 119.

Kai, K. 1986, *Solar Phys.* **104**, 235.

Kane, S.R., Fenimore, E.E., Klebasadel, R.W. and Laros, J.G. 1988, *Ap.J.*, **326**, 1017.

Kundu, M. R., and Woodgate, B. 1985, **Energetic Phenomena on the Sun**. NASA Conf. Publ. 2439.

Leach, J. 1984, Ph.D. Thesis, Stanford University.

Leach, J., Emslie, A.G. and Petrosian, V. 1985, *Solar Phys.*, **96**, 331.

Leach, J. and Petrosian, V. 1981, *Ap.J.*. **251**, 781.

Leach, J. and Petrosian, V. 1983, *Ap.J.*, **269**, 715.

Lifshitz, E.M. and Pitaevskii, L.P. 1981, **Physical Kinetics**, (Oxford: Pergamon), Ch. 2.

Lu, E.T. and Petrosian, V. 1988, *Ap.J.*, **327**, 405.

Lu, E.T. and Petrosian, V. 1989, *Ap.J.* **338**, 1122.

Lu, E.T. and Petrosian, V. 1990, (To be published in *Ap.J.* May 10,1990).

McTiernan, J.M. 1989, Ph.D. Thesis, Stanford University.

McTiernan, J.M. and Petrosian, V., 1990a, (To be published in *Ap.J.* May 1990).

McTiernan, J.M. and Petrosian, V., 1990b, (To be published in *Ap.J.* May 1990).

McTiernan, J.M. and Petrosian, V., 1991, (To be submitted to *Ap.J.*).

Miller, J.A. and Ramaty, R. 1989, *Ap.J.*, **344**, 973.

Petrosian, V. 1985, *Ap.J.*, **299**, 987.

Peterson, L. and Winckler, J. 1959, *J. Geophys. Res.* **64**, 697.

Rieger, E., Reppin,C., Kanbach, G., Forrest, D.J., Chupp, E.L. and Shares, G.H. 1984, 18th International Cosmic Ray Conference, 4), 79.
Schmahl, E., Kundu, M., and Dennis, B. 1985, *Ap.J.*, **299**, 1017.
Schlickeiser, R. 1989a, *Ap.J.*, **336**, 243.
Steinacker, J., Dröge, W., and Schlickeiser, R., 1988, *Solar Phys.*, **115**, 313.
Takakura, T. and Kai, K. 1966, *Pub. Astr. Soc. Japan*, **18**, 57.
Vestrand, W.T., Forrest, D.J., Chupp, E.L., Rieger, E., and Share, G.H. 1987, *Ap.J.*, **322**, 1010.
White, S.M., Melrose, D.G., and Dulk, G.A. 1986, *Ap.J.*, **308**, 424.

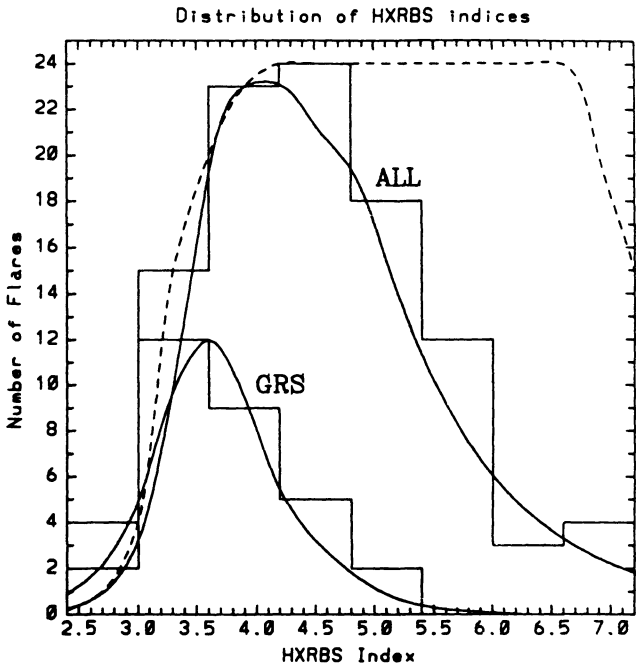

Figure 1. The distribution of hard x-ray spectral index, γ, of all flares with count rates > 1000 counts/s observed by HXRBS (histogram marked ALL) and the subset of this detected also by GRS. The two solid lines are calculated distributions assuming loops with uniform fields and accelerated electrons with power law spectral index δ. The dashed line depicts the distribution of $\delta + 1$ that gives the acceptable fits to obseervations shown.

https://doi.org/10.1017/S0074180900088306 Published online by Cambridge University Press

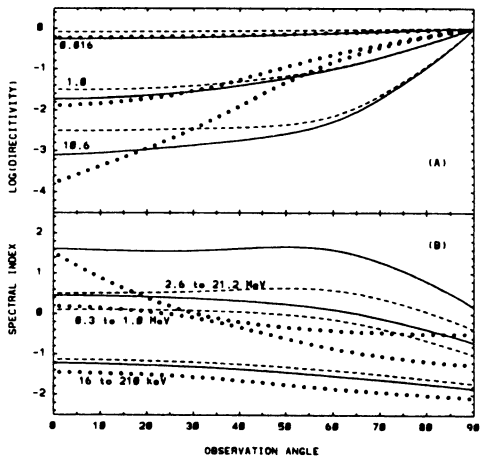

Figure 2. Directivity at the indicated photon energies in Mev (top panel) and photon spectral indices at the indicated energy range (lower panel) versus observation angle or heliocentric longitude (0 at the disk center and 90^0 at the limb). The high and low energy spectral indices are shifted up and down by one unit, respectively, for clarity. Solid lines are for uniform B field; dashed lines for a constant $d\ln B/ds$ and the dotted lines for $B \propto n^{0.2}$ with mirror ratios $b = 10$.

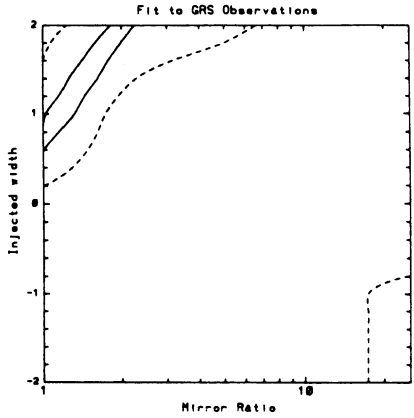

Figure 3. Constraints on the gaussian width [$\log(\alpha_o^2)$; positive for beam, 0 for isotropic and negative for pancake] of the pitch angle distribution and the degree of convergence of the magnetic field represented by the value of the mirror ratio b. The isotropic distribution is that of a model with $\alpha_o^2 = 4$ so that 1 and 2 represent $\alpha_o^2 = 0.4$ and $\alpha_o^2 = 0.04$, respectively. The area inside the solid line represents the region of the parameter space which agrees with the center-to-limb variation of the average spectral index as observed by GRS on SMM. The dashed line shows the same based on the variation of x-ray (HXRBS) to gamma-ray (GRS) flux ratio.

https://doi.org/10.1017/S0074180900088306 Published online by Cambridge University Press